EasyChair Preprint

№ 6793

Numerical Investigation on Air-Fuel Configurations on the Emission Features in a Vortex Flameless Combustion at Various Thermal Intensity

Abdelgader Agilah Gheidan, Mazlan A. Wahid, Lei Li,
Amri M. A. Wahid and Anthony C. Opia

October 7, 2021

Numerical Investigation on Air-Fuel Configurations on the Emission Features in a Vortex Flameless Combustion at Various Thermal intensity.

Abdelgader A.S. Gheidan[1, a)], Mazlan Bin Abdul Wahid[1, b)] Lei Li[1,c)], Amri M. A. Wahid[1,d)], Anthony C. Opia [1,e)]

[1]*High-Speed Reacting Flow Laboratory, School of Mechanical Engineering, Universiti Teknologi Malaysia, 81310 UTM Skudai, Johor, Malaysia*

[a)] *Corresponding author:* E-mail: *gheidan015@gmail.com*
[b)]*mazzlan@utm.my*
[c)]*ll00023@mi.wvu.edu*
[d)]*am92mzln@gmail.com*
[e)]*anthonyopia17@yahoo.com*

Abstract. A numerical study on the effects of air/fuel configuration on NOx emissions control using methane fuel combustion at different thermal intensity was conducted in this paper. The investigation employed the structure of small combustors which are influenced by some combustion factors. The layout is produced through diverse air and fuel injection configurations selected due to their potential on distinct combustion characteristics. In reverse configurations mode, the air injection port is located at the exit end of the combustor; while in the forward configurations, the air injection port is placed at the reversed end of the combustor exit, with a change of fuel position. Our investigation indicated that in both non-premixed and premixed combustion modes, the NOx discharge is extremely low. However, in premixed combustion mode, the forward and reverse flow configuration (FP, RP) premixed produced a significantly low level of NO and CO compared to the other air configurations in non-premixed at all equivalence ratios Φ. The investigation observed that any changes to the fuel injection position affect the mixture preparation, resulting in premature combustion at very low emissions, hot spots and increased emissions. The reverse-cross-flow configuration (RC1) has more potential to attain lower NO (approximately 1.30E-05 ppm) together with low CO (approximately 223 ppm) emissions when compared to the other flow configuration (RC2 and RC3). More so, a lower combustor volume leads to a very high thermal intensity of 324–393 MW/m3- atm thus resulted in a reduced residence time and gas recirculation, and high CO and NOx emissions.

INTRODUCTION

Approximately 80% of the world's electricity today is produced by the combustion method, involving various natural resources as fuel. The main resources used as the source of power generation are coal (45%), natural gas (20%) and nuclear energy (15%) respectively [1]. The primary confrontation from utilizing fossil fuel is the pollutants given off during the combustion process, leading to negative effects on the environment and human health [2,3]. Various pollutants, including unburned hydrocarbon, carbon dioxide (CO_2), carbon monoxide (CO), nitride oxide (NOx), soot, and particulate matter, are typically discharged into the air during combustion [4]. Currently, minimizing these unhealthy emissions during combustion and conserving energy are two prevailing problems faced in the creation of modern combustion systems and the energy conversion process [2]. In mitigating the aforementioned catastrophe, flameless combustion is one of the most important recent progress in combustion technology and is used in industrial furnaces that have demonstrated very low NOx performance and practised effective energy conservation [5].

Flameless combustion is created by certain techniques such as High-Temperature Air Combustion (HiTAC), Moderate or Intense Low Oxygen Dilution (MILD) combustion or Colourless Distributed Combustion (CDC) [6,7]. The structure of high thermal intensity CDC combustor needs regulation of factors including gas recirculation, fuel/oxidizer mixing, air preheats, and residence time distribution. The structure is produced through several air and fuel injection configurations selected for their potential to attain distinct combustion characteristics [8]. Various studies have been presented on how high-temperature recirculated combustion gases affect the flame [9].

The ratio of recirculated gases to fresh air stream ranged between 0% and 950%, with oxygen concentration in the hot diluted oxidizer fluctuating between 21% and 2%, respectively [10]. Progressive eddy dispersion combustion promises to be an effective technique in attaining an increased gas recirculation and intense reaction. It can be used to gain an increased residence time and thorough combustion, with little to almost no NOx emissions and constant temperature in the combustion zone [8,11]. There are a few techniques that can be utilized to enhance combustion and constancy, for instance, vortex and swirl flame. The first study on vortex flames was made by Gabler in 1998 [12] as shown in Fig. 1. Asymmetrical vortex combustor (AVC) is an innovative combustor model that can hold a constant flame over an extensive range of equivalence ratios [13]. The experiment made on ultra-reduced NO_X emissions was to investigate asymmetric compared to axisymmetric due to good mixing of air and fuel [14]. The vortex enhances the combined reactants and flame stability at the combustor inlet located at the Central Recirculation Zone (CRZ) [15]. Factors such as dilution, velocity, the position of fuel and air are all required during the combination process between fuel and air to produce effective flameless combustion [16–18]. Also, the ignition delay is needed to attain complete combustion. Ignition delay duration should be longer than the time taken to mix fuel in the oxidizer. This ensures the reactants are mixed adequately until hot recirculation gases occur [19,20]. However, for complete combustion, the combustion delay period should be shorter than the residence time in the reactor Any changes in the fuel and air injection position affects the reaction time of the mixing process, resulting in very low emission or premature ignition of hot spots and high emissions. Additionally, the position of the fuel injection significantly influences the internal recirculation rate [8,11,18,21,22]. Pre-heating air is a method that is an important part of flameless combustion. It increases the temperature in the combustion chamber, higher than that of the fuel auto-ignition. This ensures that there is adequate mixing between the fresh reactants and the hot recirculation gases, resulting in steady combustion and constant temperature, ultimately lowering the NOx emission [20,23,24]. The varying fuel and air injection configurations is a crucial factor in attaining CDC combustor. Air is either injected from the reverse end of the exit (forward flow configuration, 'F') or from the same end as exit (reverse flow configuration, 'R') [21,22]. Fuel is either injected from the same side of air injection ('S'), the opposite side of air injection ('O') or in the cross-flow ('C'). The combined air and fuel-injected results in a definitive flow configuration [8] as shown in Fig.2. Various research works have been presented on the effects of air and fuel configuration without vortex combustor flameless [21,22,25]This study goal is to investigate the effects of various air and fuel configuration on reaction in the flameless vortex combustion to achieve sufficient power at ultra-low emissions. The outcome of this study will contribute toward solving the greenhouse effect and ozone layer depletion caused by emission.

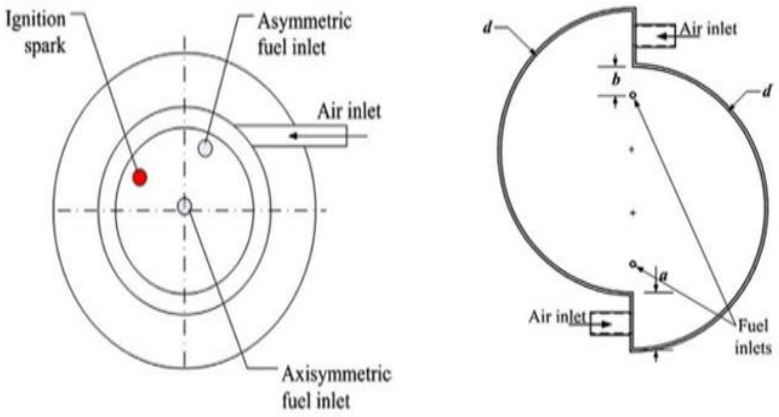

FIGURE 1. Schematic of the asymmetric vortex combustor reported by a) Gabler [12], b) Saqr [14].

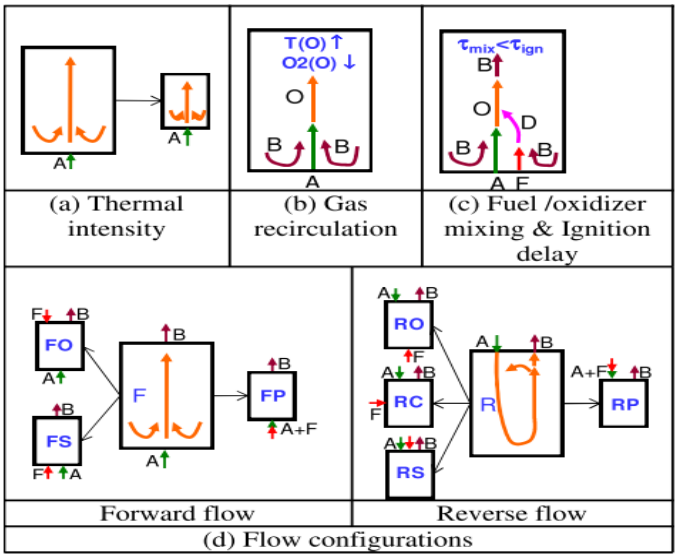

FIGURE 2. Important factors for the design of CDC combustor[8]

METHODOLOGY

COMPUTATIONAL FLUID DYNAMICS (CFD) MODELLING

The CFD developed for this numerical analysis is based on the combustor geometry used in a previous study [14,26] and uses an asymmetric combustor with tangential air inlets and axial air and fuel inlets as shown in Fig. 3. The asymmetric vortex combustor has a dimension layout; a, b, R and L of 4, 4, 15 and 45 mm respectively. The fuel and air inlet nozzles had a 1.5 mm diameter and were circular in cross-section, respectively. Exhaust gases exit the burner through a 3mm diameter central outlet. Fig. 4A shows the asymmetric chamber design of non-premixed and premixed forward air/fuel configuration. The design features six tangential air inlets and two axial fuels inlets as well as two forward axial air inlets. In forward configurations, the air injection port is located at the combustor front. The varying number of fuel injection ports produces different configurations (FS, FO and FP), as shown in Fig.4 (a), 4 (b) and 4(c). In reverse configurations, the air injection port is located at the combustor exit end. The position of fuel injection ports is changed for different configurations as shown in Fig. 4 (B). The reverse configuration has two axial air inlets and two fuel inlets on the same side as the outlet exhaust (RS), as shown in Fig. 4 (e). Fig. 4 (f) has two axial air flows inlet on the same side with the exhaust, and two fuel inlets on the opposite side of the exhaust outlet (RO). However, Fig. 4 (g) shows that reverse configuration has two air and fuel premixed flows inlet on the same side of the outlet as called (RP). Note the air tangential jet is located perpendicular to the axil fuel jet and introduces air, a full tangential velocity component into the asymmetric combustor, to improve the vortex flow in the combustion chamber. The asymmetric chamber in Fig. 5 is designed with the reversed configuration of the shifting fuel location. In the reversed configuration, the method of cross-flow (RC1, RC2 and RC3) is affected by the fuel injection location. The fuel location is adjusted in position from the air injector to achieve fuel/oxidizer mixing enhancement. Simulations are carried out in stoichiometric proportions, with 100% density of CH_4 at a temperature of 300K is calculated to be about 0.6682 Kg/m^3. The equivalence ratio is regulated by changing the inlet mass flow of air and fuel as shown in Table 1.

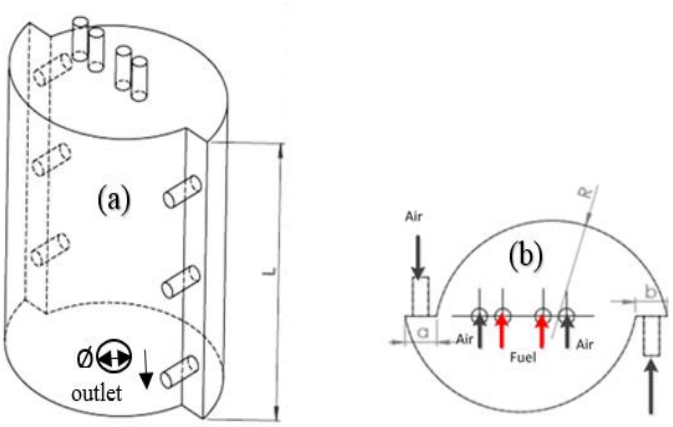

FIGURE 3. The design of mesoscale combustor flameless combustion (a) isometric view (b) top view.

TABLE 1. The equivalence ratio used

Φ	ma kg/s	mf kg/s
0.6	3.83×10^{-6}	5.37×10^{-7}
0.8	3.83×10^{-6}	7.16×10^{-7}
1	3.83×10^{-6}	8.95×10^{-7}
1.2	3.83×10^{-6}	1.07×10^{-6}
1.4	3.83×10^{-6}	1.25×10^{-6}

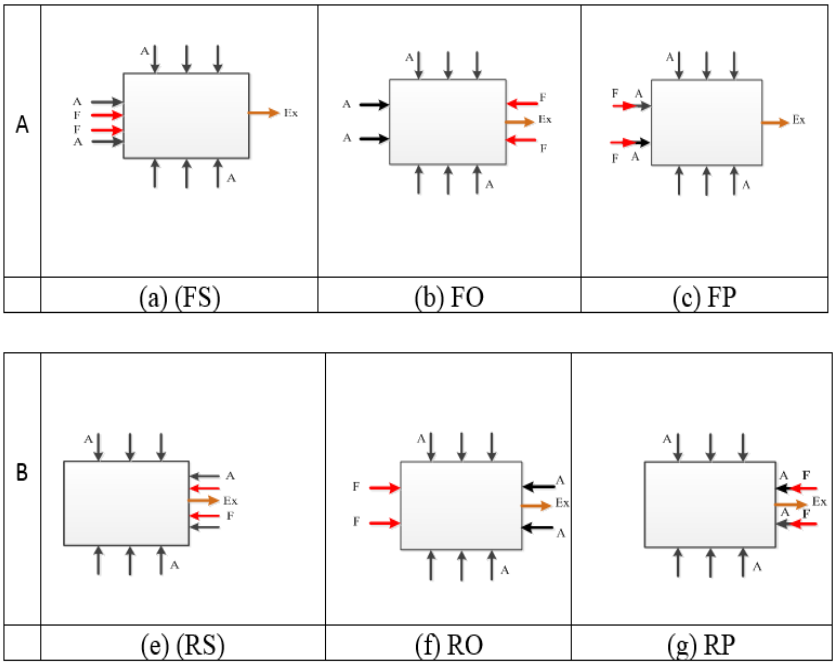

FIGURE 4. (A and B) Geometry Meso-scale vortex flameless combustion with various forward and reversed air configuration respectively.

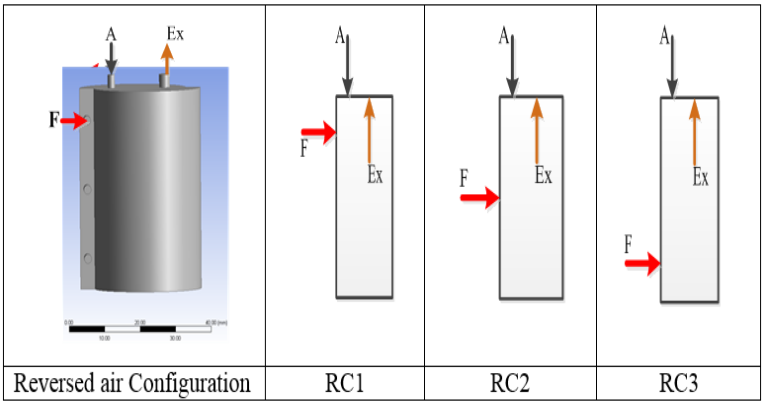

FIGURE 5. Geometry Meso-scale vortex flameless combustion with various fuel locations at reversed configuration

GOVERNING EQUATIONS

This research investigates the flameless traits of an asymmetrical vortex combustor functioning on methane at various air-fuel configurations. This section concentrates on the computational solution for constant chemically reacting vortex flows. The 3D conservation equations are given below for mass, momentum, and also energy [27–29]. The mass conservation is given as

$$u_i = \bar{u}_i + \acute{u}_i \tag{1}$$

$$\frac{\partial \rho}{\partial t} + \frac{\partial}{\partial x_i}(\rho u_i) = 0 \tag{2}$$

Where; ρ and u_i are density and flow velocity in the i-direction respectively. The momentum equation is stated as

$$\frac{\partial \rho}{\partial t}\rho u_i + \frac{\partial}{\partial x_i}\rho u_i u_j = \frac{\partial p}{\partial x_j} + \frac{\tau_{ij}}{\partial x_i} + \rho \sum_{K=1}^{N} Y_K f_{K,j} \tag{3}$$

With the viscous tensor $\tau_{i,j}$ expressed as

$$\tau_{ij} = -\frac{2}{3}\ \mu \frac{\partial u_k}{\partial x_k}\ \delta_{ij} + \mu \left(\frac{\partial_{u_i}}{\partial_{x_j}} + \frac{\partial_{u_j}}{\partial_{x_i}}\right) \tag{4}$$

Where ρ, Y_k, $f_{k,j}$ stands for the pressure, the species k mass fraction, along with the volume force that acts on the j direction of the species (k) respectively, while δ_{ij} and μ indicates the Kronecker symbol and the dynamic viscosity respectively. The energy equation is given as:

$$\rho C_p \frac{DT}{Dt} = \dot{\omega}_T + \frac{\partial}{\partial x_i}\left(\lambda \frac{\partial T}{\partial x_i}\right) - \left(\rho \sum_{K=1}^{N} C_{P,k}\, Y_k V_k\right)\frac{\partial T}{\partial x_i} + \tau_{ij}\frac{\partial u_i}{\partial x_i} + Q + \rho \sum_{K=1}^{N} Y_K f_{K,j}\ V_{kj} \tag{5}$$

Where variables C_p, T, and λ represent the mass heat capacity, the temperature, the thermal conductivity of the mixture, while $\dot{\omega}_T$, cp, k and Q is the rate of heat release, the mass heat capacity of species k, and the heat source term.

$$\frac{\partial \rho Y_k}{\partial t} + \frac{\partial}{\partial x}(\rho(u_i + V_{k,i})Y_K) = \dot{\omega}_K \quad (6)$$

Where $V_{k,i}$ and $\dot{\omega}_K$ stands for the species *k* in the direction *i* and the reaction rate of species *k* diffusion velocity respectively. Assuming all species are fixed in the gas phase, it can be conjected that the optimum gas behaviour is for all species. In this stable state of CFD simulation, methane (CH_4) is used as the fuel and the equivalence ratio is variable of non-premixed flameless combustion mode. Methane-air-2step is used to model the species transport and is calculated by the following equations [30]:

$$\mathrm{CH_4} + {}^{3}/_{2}\, O_2 \rightarrow \mathrm{CO} + 2\mathrm{H_2O} \quad \Delta\mathrm{G} = -\frac{632.68\mathrm{KJ}}{\mathrm{mol}} \quad (7)$$

$$\mathrm{CO} + {}^{1}/_{2}\, O_2 \rightleftarrows \mathrm{CO_2} \quad \Delta\mathrm{G} = -257.19\mathrm{KJ/mol} \quad (8)$$

The different equilibrium constant against the temperature can be written as Eq. (9).

$$K = \frac{\prod_j (X_j)^{vj}}{\prod_i (X_i)^{vi}} \quad (9)$$

where X_i, X_j, v_i and v_j are the molar fractions of the reactant *i*, product *j*, the stoichiometric coefficients of the reactant *i* and product *j* respectively. For the computation of Arrhenius parameters of reaction (Equation 8) is an example of the equilibrium constant K_1 and K_2 are defined as:

$$k_1 = \frac{(X_{co_2})^{v_{co2}}}{(X_{O_2})^{v_{o_2}}(X_{co})^{v_{co}}} = \frac{X^1{}_{CO_2}}{X_{O2}^{0.5} \quad X_{CO}^1} \quad (10)$$

$$k_2 = \frac{X^{0.5}{}_{o_2} X^1{}_{CO}}{X^1{}_{CO_2}} \quad (11)$$

The reaction rate is calculated by the Arrhenius equation [31].

$$k = AT^{\beta} e^{-\left(\frac{E}{RT}\right)} \quad (12)$$

Where the reaction rate, gas constant, pre-exponential and temperature are denoted by *k*, *R*, *A*, *T*, respectively while β is a dimensionless number. Assuming all species are fixed in the gas phase, it can be conjected that the optimum gas behaviour is for all species. The heat loss from the wall to the surroundings is also calculated by the equation. (13), Both thermal radiation and natural convective heat transfer are considered [32].

.

$$q = h\left(T_{s,O} - T_{\infty}\right) + \varepsilon S\left(T^4{}_{s,o} - T^4{}_{\infty}\right) \quad (13)$$

According to previous studies on macro-scale flameless combustion technology, dilution of oxidants is often referred to as one of the flameless formation fundamentals [33][34]. In Meso-flameless mode, the temperature of the inlet oxidizer (7% O_2 and 93% N_2 by vol.) is adopted 900K which is higher than the self-ignition temperature of methane.

.

NUMERICAL CONDITIONS

Flameless oxidation, colorless dispersed combustion, moderate to extreme low oxygen Dilution (MILD) combustion, and high-temperature air combustion (HiTac) are all terms used to describe flameless combustion [35–39]. In this analysis, a three-dimensional finite volume solver in FLUENT 16 is used for stable, non-mixed combustion [40]. The CFD developed for this numerical analysis is based on the geometry combustion of a previous study by Saqr [14]. The simulations are focused on the flow field profile, temperature profile, and emissions of the combustor under methane compositions at various equivalence ratios (Φ). The spatial discretization of the mass, momentum, and energy transportation equations, is based on the upwind second-order scheme. In discrete momentum equations, the SIMPLE algorithm is utilized for combinations of pressure velocity. Volumetric chemical processes are designed closely to the methane-2 phase with the k–$\boldsymbol{\varepsilon}$ method as the viscous model reaction procedure. Turbulent-chemical interactions are created with eddy dissipation equations in a previous study [41,42]. Thermal NOx calculation uses the partial equilibrium model to predict the O radical concentration required. The boundary conditions are picked according to the previous macro-scale flameless mode experiments [1]. The running pressure and temperature are 0.5 bar and 300K respectively. The temperature of the inlet oxidizer (case: 7% O_2 and 93% N_2 by vol.) is adopted in the Meso-flameless mode, 900 K, higher than the methane self-ignition temperature. Table 2 depicts the boundary conditions for the inlet oxidant. Table 3 shows the boundary conditions for the fuel inlet, wall and pressure outlet, while the general simulation is illustrated in Table 4. To calculate the approximate O_2 radical concentrations needed for thermal NOx prediction, partial equilibrium models were used. In subsequent iterations, if the residual in each equation is less than $1x10^{-6}$, the solution is determined to be concentrated as calculated through grid independence tests. M3=405,827 cells with a minimum cell size of 0.003 mm per grid independence test as shown in Fig 6. The residence time profile gathered from numerical simulations is studied in the case of a perfectly stirred reactor. The residence time (t_{res}) for a perfectly stirred reactor is obtained by Eq. (14)

$$Residence\ time = t_{res} = {}^{pv}/_{m} \tag{14}$$

Where; *P*=average gas density in a combustor, *V*=combustor volume, *m*=total mass flow rate through the combustor.

TABLE 2. The boundary condition of inlet oxidant

Oxidizer inlet	**Value**
Temperature	$T_{inlet\ air}$ = 300 K
Gauge Pressure	0
Hydraulic diameter	2mm
Turbulent intensity	10
Oxygen concentration	7%
Density (ρ) Kg/m^3	ρ= 1.16 kg/m^3

TABLE 3. The boundary condition of fuel inlet, wall and pressure outlet

	Boundary conditions	
Fuel inlet	Temperature	$T_{inlet\ fuel}$ = 300
	Gauge pressure	0
	Hydraulic diameter	3
	Turbulent intensity	10
	Fuel	CH_4
	Density	0.6682 Kg/m^3
	Mass flow rate	Variable
Wall	Wall slip	Non-slip
	Material	Steel
	Heat transfer confection	5 $w/m^2 k$
Pressure outlet	Hydraulic diameter	3mm
	Gauge pressure	0
	Turbulent intensity	5

TABLE 4. Initial Settings of simulation

Steps	
Viscous model	k–e Standard
Radiation model	Discrete ordinate (DO)
Combustion model	Species transport / partially premixed combustion
Mixture properties	Methane–air
Turbulence chemistry interaction	EDM Volumetric
Reaction	Thermal NOx
NOx	Prompt NOx

The grid independence test was performed to discretize the flow domain as illustrated in Fig6. Fig 7 shows the plots of central axis temperature along with the axial position for four various meshes. M1 consists of 173,212 cells, while M2 consists of 200,282 cells. Tetrahedral elements were used to make M3=405,827 cells and M4=650,381 cells. Since the needed computation time is still tolerable given the capacity, the final mesh with M3 was chosen for subsequent simulation runs.

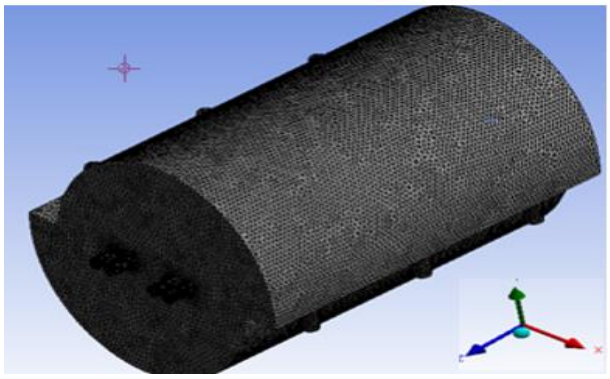

FIGURE 6. Mesh Meso-scale flameless combustion.

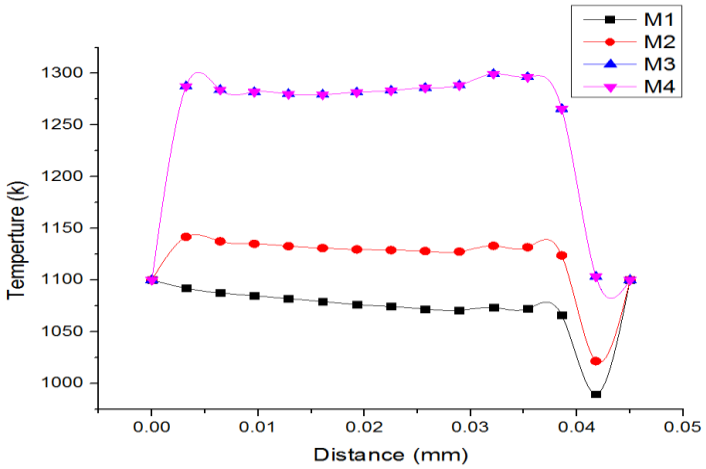

FIGURE 7. Grid independence test.

MODEL VALIDATION

The model validation performed was associated with the geometry and boundary conditions, used by Wu et al. [43]. Air goes into the asymmetric combustor (300K) with full tangential velocity. The combustor comprises six tangential air flows, two axial air and two axial fuel inlets. Fuel component was conducted at a ratio of equal to Φ = 1. The mass flow rate of the air inlet was set at $3.83x10^{-06}$ kg/s. Reactions were conducted based on the different turbulence structures to compare the experimental results with K-epsilon (2 Eq) RNG was picked as the turbulence model. The validity of the code was taken when compared with the results of other turbulence models which were experimentally associated and produced according to Saqr and Khaleghi [44,45]. Extremely little NOx concentrations were identified in both the premixed and non-premixed combustion modes. The current study is compared with the experimental records, thereby confirming that the simulated results are reliable, similar to the presentations by [8,39,46–48]. The forward flow premixed configuration FP created a substantially lesser number of NO and CO emissions in comparison to other air configurations (RS, FO and FS) at all identical ratios Φ, similar to the findings by [8,46]. The results also show that NOx and CO emission levels of forward configuration (FS) is lesser than configuration (FO) at an equivalence ratio of Φ=0.6 to 1.4 in line with previous studies observation [8,39] Additionally, the results suggested that NOx and CO emission level of reversed configuration (RS) is lesser than configuration (RO) by the data collated, explained the same with past reports [8][49]. The current study shows the differences in NOx emission circulation factored by the change fuel position as compared to the previous experiment [8,11,22]. Residence time and gas recirculation are also further decreased when the combustor is running at an increased thermal intensity, leading to an increase in CO and NOx emissions. This is the same with past presentations [8,21].

RESULTS

EFFECT OF AIRFLOW CONFIGURATION FORWARD ON NOX EMISSIONS

Fig. 8 shows the airflow design, tested on the forward airflow configuration in non-premixed and premixed at the various air and fuel inlets. The test analysed the impact of NOx pollution resulting from flameless vortex combustion. In the FS and FP configuration as the equivalence ratio increases, NOx emission was found to be significantly lowered from Φ=0.6 until to Φ=1.4. In the FO configuration, NOx emission was found to rise sharply from Φ=0.6 until Φ=1.4, reaching (5.20E-03ppm) at Φ=1.4. NOx emission level in the FS configuration is lesser than the FO configuration at Φ=0.6 to Φ=1.4. NOx emissions were observed to be lower in premixed configuration FP than in non-premixed configurations FS and FO, recorded the same

result on previous presentation [21,39]. In FO configuration, the CO behaviour was found to be more active as the equivalence ratio increases up to 529 ppm at Φ=1.4. CO starts to slowly decrease in FS configuration from 327 ppm at Φ=0.6 to 285 ppm at Φ=1.4.

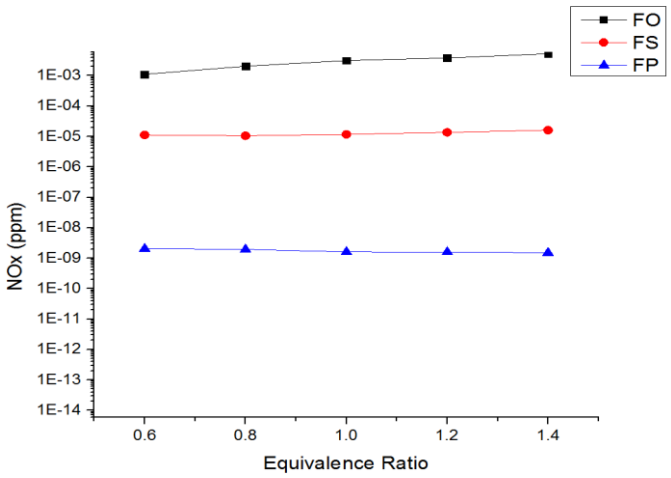

FIGURE 8. Effects of Equivalence ratio on NOx emissions at forward flow configuration.

In the FP premixed configuration, CO starts to lessen slowly till it hits 102 ppm at Φ=1.4 as indicated in Fig. 9. In conclusion, the CO emission level in the FS configuration is lesser than in the FO configuration at all equivalence ratios. The least amount of CO emissions was observed at FP configuration in premixed combustion modes instead of the non-premixed configuration FS & FO, at an equivalence ratio from Φ=0.8 to 1.4, similar to work presented previously [8,39].

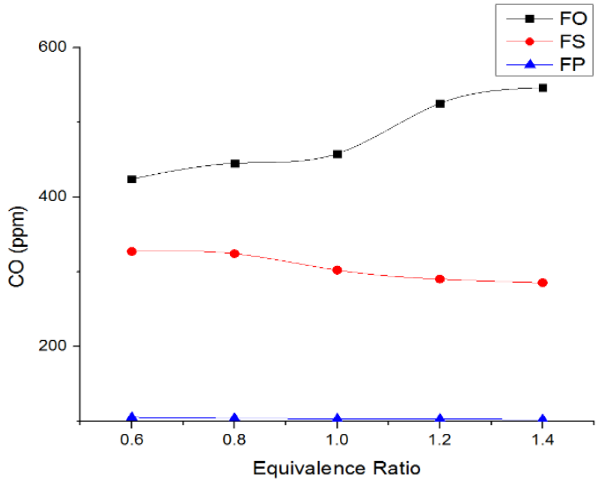

FIGURE 9. Effects of Equivalence ratio on CO mass fraction at forward flow configuration.

Fig. 10 depicts the volumetric temperature distribution inside the chamber in flameless combustion for various forward configurations (T = 300 K, Oxygen concentration = 7%), as well as the concentration of various species of combustion reactants for various configurations to create NOx. In multicomponent systems, the species distribution is the product of a chemical reaction as well as the mass transport mechanism.

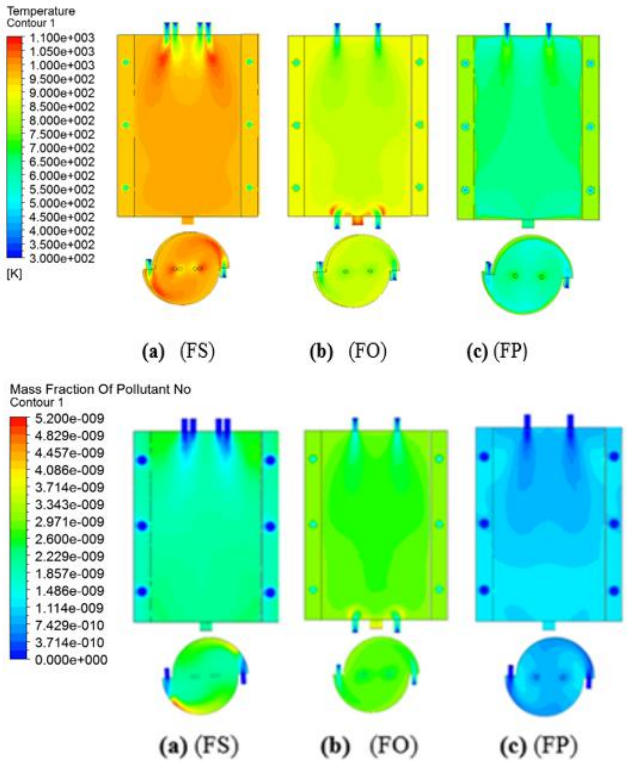

FIGURE10. Geometry mesoscale vortex flameless combustion with various forward air configurations (a) FS (b) (FO), (c) (FP) on Temperature and NOx emission at (Φ=1).

EFFECT OF AIRFLOW CONFIGURATION REVERSED ON NOX EMISSIONS

In RP configuration results as in Fig. 11, as the equivalence ratio increases, the NOx level was found to be lowered significantly from Φ=0.6 to Φ=1.4. In RS configuration, NOx emission was observed to diminish considerably from (1.59E-04 ppm) at Φ=0.6 to (1.50E-04 ppm) at Φ=0.8, before rising to (2.42E-04ppm) at Φ=1.4. In contrast, RO configuration saw a gradual decrease from (1.50E-05ppm) at Φ=0.6 to (1.44E-05 ppm) at Φ=1, before rising to (2.23E-05ppm) at Φ=1.4. In conclusion, NOx emission in RO configuration is substantially lesser than RS configuration, stated the same on presentations [8,49]. The lowest NOx emission was identified in RP premixed configuration instead of RS and RO non-premixed configuration [8,49]. CO emissions were seen to increase from Φ=0.6 to Φ=1.4 for both RS and RO cases. In RP configuration, CO emissions are seen to be decreased when the equivalence ratio rises. The CO emissions in RS configuration fluctuates when the equivalence ratio increased to 426 ppm at Φ = 1.4. In RO configuration, CO starts to rise steadily from 251 ppm at Φ=0.6 to 305 ppm at Φ=1.4. For RP configuration, CO emission starts to rise gradually at 102 ppm at Φ=0.6, before decreasing to 85 ppm at Φ=1.4. The RO non-premixed configuration has the potential to attain lower NO and CO emissions compared to the RS configuration [8,49]**.** RP premixed configuration (RP) has more promise to attain lower NO and CO emission compared to RS and RO configurations, supported by past studies [8,22].

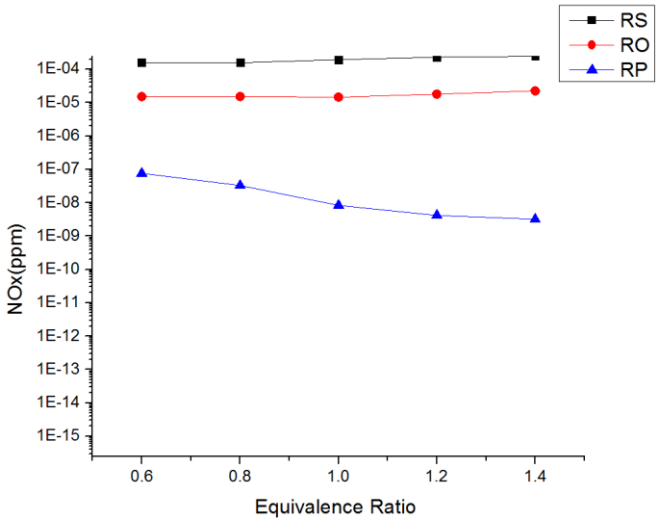

FIGURE 11. Effects of Equivalence ratio on NOx emissions at forward flow configuration.

Fig. 12**,** concluded that the CO emission level in RO configuration is substantially lesser than RS. The lowest CO emission was seen in RP premixed combustion instead of RS and RO non-premixed configuration. Fig. 13 depicts the volumetric temperature distribution within the burner during flameless combustion for various reversed flow configurations (T=300K, oxygen concentration = 7%), as well as the various types of combustion reactants used to produce NOx emissions.

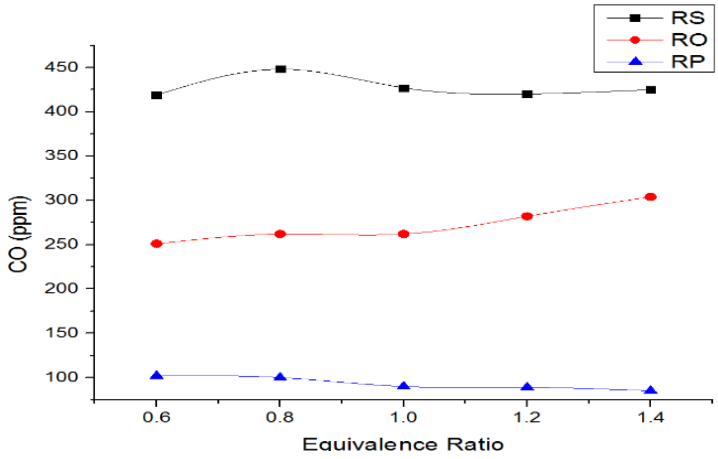

FIGURE. 12 Effects of Equivalence ratio on CO mass fraction at Reverse flow configuration

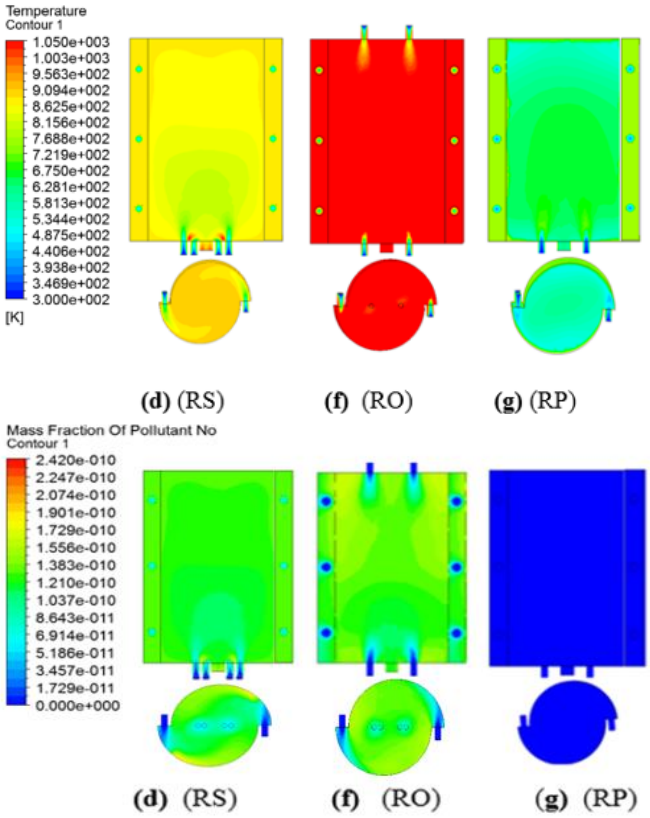

FIGURE 13. Geometry mesoscale vortex flameless combustion with various Reversed air configuration (d) (RS), (f) (RO) and (g) (RP) on Temperature and NOx emission at (Φ=1).

EFFECT OF FUEL LOCATION ON NOX EMISSIONS IN AIRFLOW REVERSED CONFIGURATION

Fig. 14 and 15 described the reverse flow configuration in cross-flow based on fuel location (see Fig. 5), RC1 Configuration had the very lowest NO (about 1.30E-05 ppm) and CO (about 223 ppm) emissions as compared to RC2 and RC3. Additionally, the length between the air and fuel injection ports affects the combustor behaviour. If the fuel injection is positioned further from the air injection, the ignition delay will be brief and combust before the fuel is thoroughly mixed, resulting in a rise of emitted NO and CO. If the fuel injection is positioned closer to the air injection port, the fuel/oxidizer mixing is improved, resulting in lesser emitted NO and CO, supported by the previous works [8,11,22]. The RC1 non-premixed configuration has a lot of potentials to attain lower NOx and CO gas is given off due to encouraging flameless combustion traits.

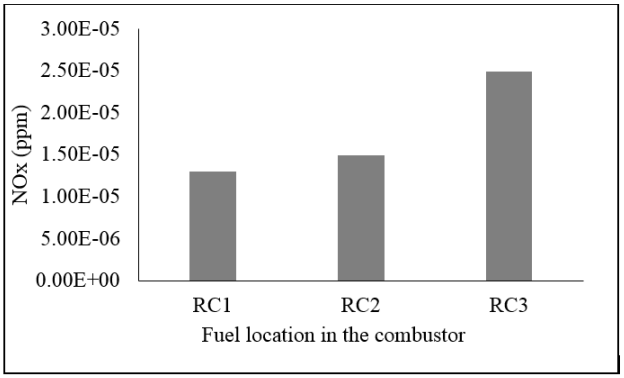

FIGURE 14. Effects of inlet fuel location on NOx emissions in reversed air configuration at (Φ=1).

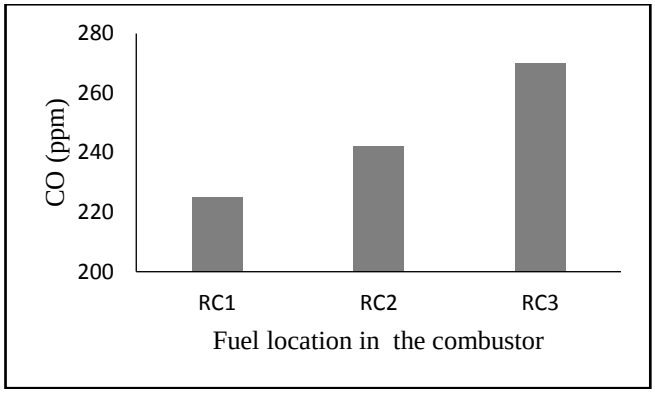

FIGURE 15. Effects of inlet fuel location on CO emissions in reversed air configuration at (Φ=1).

EFFECT OF THERMAL INTENSITY VARIATION ON NO_X EMISSION

In thermal Intensity, the level of heat or energy is given off are calculated by the quantity of heat energy emitted per unit, measured in a combustor unit volume, adjusted by the operating pressure. The unit of thermal strength is MW/m^3-atm. Thermal Intensity is a representation of the residence time of gases in the combustor [50,51]. However, numerous complications due arise such as attaining flame stabilisation, higher flow rates and hitting the peak fuel conversion. The complications are due to the duration required for mixing and full combustion must be shorter than the time needed for a residence. The process of converting carbon monoxide takes a long time. The reduced residency time will lead to an increase in CO levels[39,50,51]. The structure requirement for combustor applications differs because of the high thermal strength and pressure operation that significantly lowers residence time [52]. To prevent the effects of fuel/air mixing on combustion, these combustors are studied for the effects of thermal intensity on NOx and CO emissions in a premixed simulation. In most studies, the inlet temperature of the air and fuel mixture was kept at a constant 300 K. Fig. 4A(a) analyzed the forward flow configurations at the thermal intensity of 65-324 MW/m^3-atm, with FS configuration utilized. As mentioned earlier, the combustor size fluctuates caused by a fuel injection mass flow rate at $8.95x10^{-07}$ kg/s and air injection mass flow rate at $3.83x10^{-06}$ kg/s at an equivalence ratio of 1. Combustions occur at a higher thermal intensity, within the range of 65-324MW/m^3-atm. Emission concentration was calculated at an equivalence ratio of 1.

Fig. 16 shows the emitted NO and CO levels at the thermal intensity range of an equivalence ratio of 1. NO emissions are found to be very low (less than 8E-04 ppm) in all studies done. However, NO emission rises in rising thermal intensity, possibly due to the approximately lesser heat losses at higher thermal intensity. This led to an

increased gas temperature and subsequently, an increase in NO and CO emissions [52]. At the thermal intensity of 65 MW/m^3-atm, CO given off is only 279 ppm, whereas, at a thermal intensity of 183 MW/m^3-atm, CO emitted rose to 330 ppm, and 349 ppm at a thermal intensity of 324 MW/m^3-atm. Take note that the air injection temperature, injection mass flow rate and injection diameter, is kept constant in all three tests done. The rise in CO is suggested to be due to the decreased residence time at increased thermal intensities as shown in Fig. 17 (a) and (b).

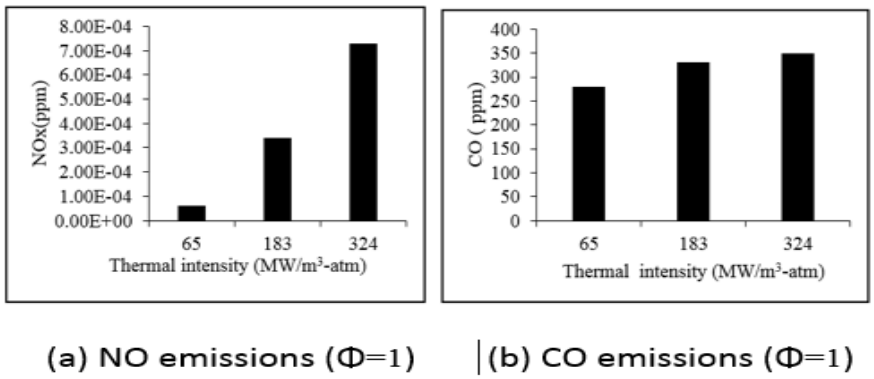

FIGURE 16 (a) NO, and (b) CO emissions for forward flow mode corresponding to a thermal intensity range of 65–324 MW/m^3-atm.

Fig. 17 (a) and (b) show the effects of thermal strength on residence time and CO emissions. CO oxidation is a time-consuming process in all combustion operations. Therefore, lesser residence time results in more CO emission levels. Fig. 17 (b) suggests that a stronger thermal intensity relates to a lesser residence time, leading to an increase in CO emissions

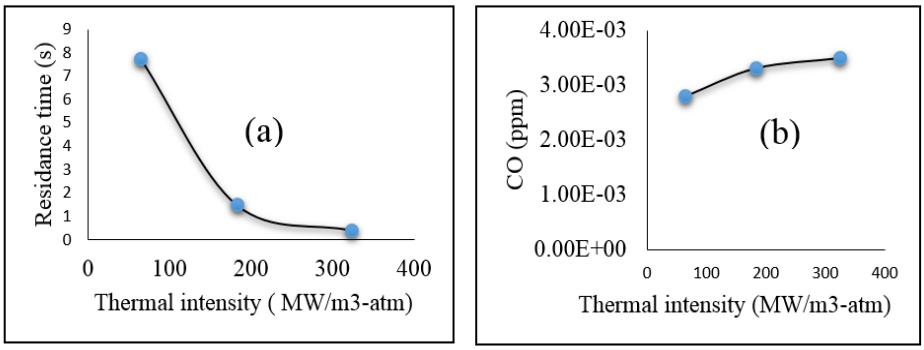

FIGURE 17. Effect of thermal intensity on (a) average residence time and (b) CO emissions (perfectly stirred reactor, Φ=1) for forward flow mode

An increase in heat intensity results in decreased residence time. This is because of the increase in the volumetric flow of air and fuel for the same heat load. For example, the thermal intensity of 65MW/-m^3-atm has a residence time of 7.7s, while the thermal intensity of 183 MW/-m^3-atm has a residence time of 1.5s. CO emission of about 279 ppm happens at 65 MW/m^3-atm while emission of 331 ppm occurs at 183 MW/m^3-atm. The mean residence time for the various combustors is shown in Fig. 17, which suggests that the residence time goes down from 7.70 s to 0.38 s when the thermal intensity rises from 65 to 324 MW/m^3-atm. The residence time was calculated at an equivalence ratio of 1. In conclusion, it can be said that combustors with stronger thermal intensity have lesser residence time, leading to an increase in CO emissions (see Fig. 17 (b)).

The reverse flow configurations were studied at a thermal intensity of 81-393 MW/m^3-atm (see Fig. 4 B (e)) with RS configuration utilized. Similar to forward combustor configuration, the combustor size fluctuates caused by a fuel injection mass flow rate at 8.95x10^{-07} kg/s and air injection mass flow rate at 3.83x10^{-06} kg/s at an equivalence ratio of 1. Fig. 18 shows NO and CO emission at a thermal intensity of 81-393 MW/m^3 atm. The NO (less than (1.150E-04

ppm) and CO (less than 436 ppm) given off is very low. However, the NOx level rises when thermal intensity gain strength. This can be due to the decrease in heat losses at stronger thermal intensity, leading to an increase in gas temperatures and consequently, an increase in NO emitted. There is a substantial difference in CO levels in reversed flow[8]. Fig. 19 (a) depicts varying combustors with the mean residence time decreasing from 6 s to 0.3 s when thermal intensity is increased from 81 to 393 MW/m^3-atm. The residence time was calculated at an equivalence ratio of Φ=1. At the thermal intensity of 81MW/m^3-atm, CO emitted is only 436 ppm and it rises to 479 ppm when thermal intensity is at 196 MW/m^3-atm. CO emission is at 440 ppm when thermal intensity is at 393 MW/m^3-atm. **Fig. 19** (b) shows substantial differences in CO emitted in reversed flow configurations. In contrast, Fig. 17 (b) shows the CO emissions rising with stronger thermal intensity in forward flow configuration.

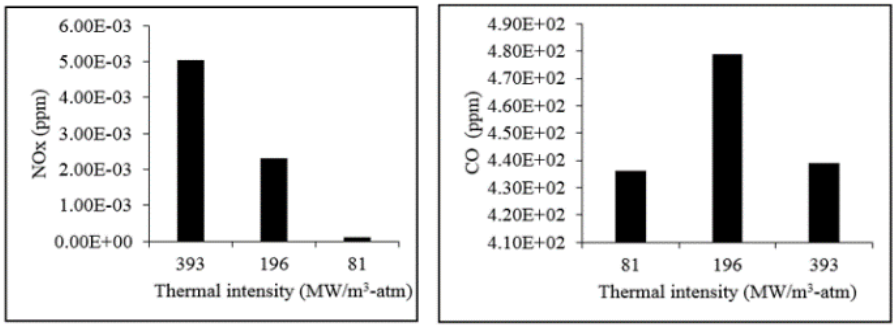

(a) NO emissions (Φ=1) (b) CO emissions (Φ=1)

FIGURE 18. Emissions for reversed flow mode corresponding; NO (a), and CO (b) to a thermal intensity range of 81–393 MW/m3-atm at (Φ=1).

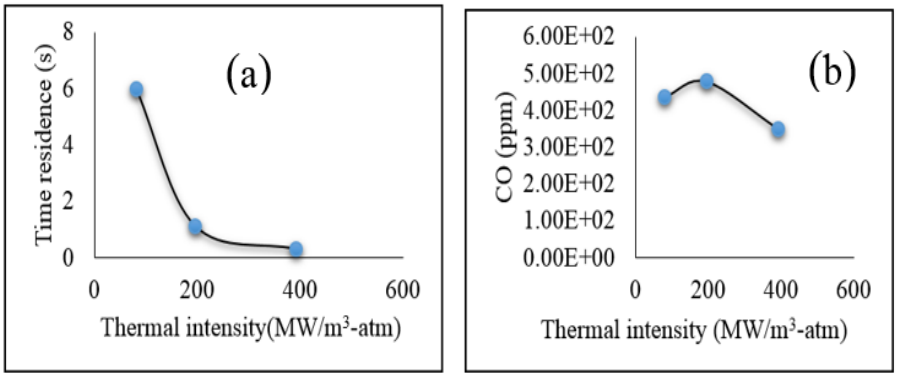

FIGURE.19. Effect of thermal intensity on (a)average residence time and (b) CO emissions (perfectly stirred reactor, Φ=1) for reversed flow mode.

CONCLUSIONS

To produce flameless combustion in asymmetric vortex operation, a detailed assessment of the various inputs and process guidelines for minimal NOx emission to minimize pollution is needed. Two flow premixed and four non-premixed configurations of different variations were assessed with algorithmic simulations to pick the optimum structure that gives off the least NOx. These assessments concluded that substantial internal recirculation of gases was reliant on the design of an asymmetric vortex combustor. These assessments also presented very low NOx gases for varying combinations of air and fuel configuration in a flameless asymmetric vortex as compared to the previous study. The differences between fuel injection and different directions of air influences mixture formation resulting in early combustion occurring with very low emissions or hot spots with increased emissions. Each combustor has two types of air configuration: forward flow and reversed flow in premixed and non-premixed modes. Extremely low NOx emissions were identified in both the premixed and non-premixed combustion. However, the forward flow premixed configuration (FP, RP) produced a significantly lower level of NOx and CO emissions as compared to other air configurations (RS, RO, FO and FS) at all equivalence ratios Φ. This can be attributed to an efficient mixing between

the fuel and oxidizer, leading to an increased residence time of the created gases inside the combustor. The forward flow configuration "FS, FP" resulted in very low NOx (about (4.50E-05ppm) ppm in non-premixed and (6.50E-09ppm) ppm in premixed) and CO emissions (285 ppm in non-premixed and 102 ppm premixed). The reversed flow configuration "RO" achieved minimal NOx at approximately (1.44E-05 ppm) in non-premixed at Φ=1 and CO emissions 251 ppm at Φ=0.6. The reversed-cross-flow configuration (RC1) has the potential to achieve lesser NOx and CO emissions compared to other configurations (RC2 and RC3). As the fuel injection location was placed further below away from air injection for the cross-flow modes, NOx and CO that are given off rises, probably due to lower mixing and residence time. It was found that the operation of the combustor at an increased thermal intensity lead to a decreased residence time and gas recirculation. Still, in reversed configuration results, there is a substantial variation in CO emissions.

NOMENCLATURE

CFD	Computational Fluid Dynamics
AVC	Asymmetrical vortex combustor
CRZ	Central Recirculation Zone
F	Forward flow configuration
R	Reverse flow configuration
P	Premixed flow configuration

Greek symbols

ρ	density
t_{res}	residence time

Subscripts

Φ	Equivalence ratios
q	Mass of heat transfer
K	Reaction rate
E	Exit

REFERENCE

1. S. E. Hosseini and M. A. Wahid, "Enhancement of exergy efficiency in combustion systems using flameless mode," *Energy Convers. Manag.*, 86, 1154–1163 (2014).
2. A. A. Abuelnuora, M. A. Wahida, A. Saata, "Characterization of a Low NO x Flameless Combustion Burner Using Natural Gas," *J. Teknol.*, 2 (x) 121–125 (2014).
3. S. E. Hosseini, M. A. Wahid, and N. Aghili, "The scenario of greenhouse gases reduction in Malaysia," *Renew. Sustain. Energy Rev.*, 28 (12) 400–409 (2013).
4. A. A. Abuelnuor, M. A. Wahid, H. A. Mohammed, and A. Saat, "Flameless combustion role in the mitigation of NOx emission : a review," Int. J. ENERGY Res., 38(x) 827–846 (2014).
5. A. Milani and J. G. Wünning, "Flameless Oxidation Technology," *Adv. Combust. Aerothermal Technol.*, 343–352 (2007).
6. G. De Azevedo, C. De Andrade, and F. D. S. Costa, "Flameless compact combustion system for burning hydrous ethanol," *Energy*, 89, 158–167 (2015).
7. J. S. Feser, S. Karyeyen, and A. K. Gupta, "Flowfield impact on distributed combustion in a swirl assisted burner," *Fuel*, 263(11) 116643 (2020).
8. V. K. Arghode and A. K. Gupta, "Role of thermal intensity on operational characteristics of ultra-low emission colorless distributed combustion," *Appl. Energy*, 111, 930–956 (2013).
9. A. K. Gupta and T. Hasegawa, "The effect of air preheat temperature and oxygen concentration in air on the structure of propane air diffusion flames," *37th Aerosp. Sci. Meet. Exhib.*, 121 (9) 209–216 (1999).

10. A. E. E. Khalil and A. K. Gupta, “Swirling flowfield for colorless distributed combustion,” *Appl. Energy*, 113 (x) 208–218 (2014).
11. A. E. E. Khalil and A. K. Gupta, “Swirling distributed combustion for clean energy conversion in gas turbine applications,” *Appl. Energy*, 88(11) 3685–3693 (2011).
12. H. C. Gabler, *An experimental and numerical investigation of asymmetrically-fueled whirl flames* . (1998).
13. K. M. M. E. M. Saqr., “Aerodynamics and Thermochemistry of Turbulent confined Asymmetric Vortex Flames. A thesis submitted in fulfillment of the requirements for the award of the degree of Doctor of Philosophy (Mechanical Engineering),” (2011).
14. K. M. Saqr, H. S. Aly, M. M. Sies, and M. A. Wahid, “Computational and experimental investigations of turbulent asymmetric vortex flames,” *Int. Commun. Heat Mass Transf.*, 38(3) 353–362 (2011).
15. M. S. A. Ishak and M. N. Mohammad, “Effect of velocity variation at high swirl on axial flow development inside a can combustor,” J. Teknol., 71(2) 19–24 (2014).
16. A. E. E. Khalil and A. K. Gupta, “The role of CO2 on oxy-colorless distributed combustion,” *Appl. Energy*, 188, 466–474 (2017).
17. A. S. Veríssimo, A. M. A. Rocha, and M. Costa, “Importance of the inlet air velocity on the establishment of flameless combustion in a laboratory combustor,” *Exp. Therm. Fluid Sci.*, 44, 75–81 (2013).
18. S. Sharma, H. Pingulkar, A. Chowdhury, and S. Kumar, “A new emission reduction approach in MILD combustion through asymmetric fuel injection,” *Combust. Flame*, 193, 61–75 (2018).
19. P. Sabia, M. de Joannon, M. Lubrano Lavadera, P. Giudicianni, and R. Ragucci, “Autoignition delay times of propane mixtures under MILD conditions at atmospheric pressure,” *Combust. Flame*, 161(12) 3022–3030 (2014).
20. G. Sorrentino, P. Sabia, M. De Joannon, and P. Bozza, “Influence of preheating and thermal power on cyclonic burner characteristics under mild combustion,” 233(6) 207–214 (2018).
21. V. K. Arghode and A. K. Gupta, “Investigation of forward flow distributed combustion for gas turbine application,” *Am. Soc. Mech. Eng. Power Div. POWER*, vol. 88(1) 57–70 (2010).
22. V. K. Arghode and A. K. Gupta, “Investigation of reverse flow distributed combustion for gas turbine application,” *Appl. Energy*, vol. 88(4) 1096–1104 (2011).
23. S. Prabakaran, J. Fournier, and O. Le Corre, “A comparative study of methane MILD combustion in O2/N2, O2/CO2 and O2/H2O,” *Energy Procedia*, 158, 1473–1478 (2019).
24. M. Mehregan and M. Moghiman, “A numerical investigation of preheated diluted oxidizer influence on NOx emission of biogas flameless combustion using Taguchi approach,” *Fuel*, vol. 227 (7) 1–5 (2018).
25. V. K. Arghode and A. K. Gupta, “Effect of confinement on colorless distributed combustion for gas turbine engines,” 45th AIAA/ASME/SAE/ASEE Jt. Propuls. Conf. Exhib., 2 (8) 1–10 (2009).
26. C. G. Abler, “An Experimental and Numerical Investigation of Asymmetrically-Fueled Whirl Flames," PhD, , Princeton University, Princeton University,” (1998).
27. K. M. Saqr, H. S. Aly, M. A. Wahid, and M. M. Sies, “Numerical simulation of confined vortex flow using a modified k-ε turbulence model,” *CFD Lett.*, 1 (2) 87–94 (2009).
28. K. M. Saqr, H. S. Aly, H. I. Kassem, M. M. Sies, and M. A. Wahid, “Computations of shear driven vortex flow in a cylindrical cavity using a modified k-ɛ́ turbulence model,” *Int. Commun. Heat Mass Transf.*, 37(8) 1072–1077 (2010).
29. M. M. Sies and M. A. Wahid, “Numerical investigation of the asymmetrical vortex combustor running on biogas,” *J. Adv. Res. Fluid Mech. Therm. Sci.*, 74(1) 1–18 (2020).
30. F. L. Dryer and C. K. Westbrook, “Simplified Reaction Mechanisms for the Oxidation of Hydrocarbon Fuels in Flames,” *Combust. Sci. Technol.*, 27 (1–2) 31–43 (1981).
31. J. H. Tien and R. J. Stalker, “Release of chemical energy by combustion in a supersonic mixing layer of hydrogen and air,” *Combust. Flame*, 131(3) 329–348 (2002).
32. G. Bagheri, E. Hamidi, M. A. Wahid, A. Saat, and M. M. Sies, “Effects of CO_2 dilution on the premixed combustion of CH4 in microcombustor,” *Appl. Mech. Mater.*, 388, 251–256 (2013).
33. S. E. Hosseini, G. Bagheri, and M. A. Wahid, “Numerical investigation of biogas flameless combustion,” *Energy Convers. Manag.*, 81, 41–50 (2014).
34. B. Danon, E. S. Cho, W. De Jong, and D. J. E. M. Roekaerts, “Numerical investigation of burner positioning effects in a multi-burner flameless combustion furnace,” *Appl. Therm. Eng.*, 31 (17–18). 3885–3896 (2011).
35. S. E. Hosseini, M. A. Wahid, and A. A. A. Abuelnuor, “Biogas Flameless Combustion : A Review,” *Appl. Mech. Mater.*, 388, 273–279 (2013).
36. M. Katsuki and T. Hasegawa, “The science and technology of combustion in highly preheated air,” *Symp.*

Combust., 27(2) 3135–3146 (1998).
37. I. B. Özdemir and N. Peters, "Characteristics of the reaction zone in a combustor operating at mild combustion," *Exp. Fluids*, 30(6) 683–695 (2001).
38. J. A. Wuenning and J. G. Wuenning, "Flameless Oxidation to Reduce Thermal {NO}-formation," *Prog. Energy Combust. Sci.*, 23, 81–94, (1997).
39. V. K. Arghode and A. K. Gupta, "Development of high intensity CDC combustor for gas turbine engines," *Appl. Energy*, 88(3) 963–973 (2011).
40. "'ANSYS Fluent Theory Guide Release 16.0, SAS IP.' Inc 894 -895 (2015): .
41. J. P. Kim, U. Schnell, and G. Scheffknecht, "Comparison of different global reaction mechanisms for MILD combustion of natural gas," *Combust. Sci. Technol.*, 180 (4) 565–592 (2008).
42. B. F. Magnussen and B. . Hjertager, "On mathematically modeling with special emphasis on soot formation and combustion," 16(8) 719–729 (1977).
43. M. H. Wu, Y. Wang, V. Yang, and R. A. Yetter, "Combustion in meso-scale vortex chambers," *Proc. Combust. Inst.*, 31, 3235–3242 (2007).
44. M. Khaleghi, S. E. Hosseini, and M. A. Wahid, "Emission and combustion characteristics of hydrogen in vortex flame," *J. Teknol. (Sciences Eng.*, 66 (2) 47–51 (2014).
45. K. M. Saqr, H. S. Aly, M. M. Sies, and M. A. Wahid, "Effect of free stream turbulence on NOx and soot formation in turbulent diffusion CH_4-air flames," *Int. Commun. Heat Mass Transf.*, 37 (6) 611–617, 2010.
46. V. K. Arghode and A. K. Gupta, "Investigation of forward flow distributed combustion for gas turbine application," *Appl. Energy*, 88 (1) 29–40 (2011).
47. V. K. Arghode and A. K. Gupta, "Hydrogen addition effects on methane-air colorless distributed combustion flames," *Int. J. Hydrogen Energy*, 36(10) 6292–6302 (2011).
48. A. E. E. Khalil, V. K. Arghode, and A. K. Gupta, "Novel mixing for ultra-high thermal intensity distributed combustion," *Appl. Energy*,105, 327–334 (2013).
49. V. K. Arghode and A. K. Gupta, "Effect of flow field for colorless distributed combustion (CDC) for gas turbine combustion," *Appl. Energy*, 87 (5) 1631–1640 (2010).
50. A. E. E. K. Hasan, "Investigation of Colorless Distributed Combustion (CDC) with Swirl for Gas Turbine Application," 1-370 (2013).
51. V. K. Arghode, "Development of colorless distributed combustion for gas turbine application (Doctoral dissertation).," 1- 303 (2011).
52. V. K. Arghode, A. E. E. Khalil, and A. K. Gupta, "Fuel dilution and liquid fuel operational effects on ultra-high thermal intensity distributed combustor," *Appl. Energy*, 95 (3) 132–138 (2012).